ADVANCED FUNCTIONAL MATERIALS
www.afm-journal.de

Engineering a Single Amino Acid Bionanozyme for Ultrasensitive Detection of Biomarkers: A WHO-REASSURE-Aligned Approach

Subrat Vishwakarma, Om Shanker Tiwari, Vijay Kumar Patel, Ruchi Shukla, Ehud Gazit, and Pandeeswar Makam**

The development of advanced biosensing materials that adhere to the WHO-REASSURE standards is crucial in resource-constrained environments. Conventional peroxidase (POD) enzymes, essential for sensitive and selective colorimetric assays, encounter challenges such as high production costs, operational instability, complex fabrication processes, and non-reusability. In response to these challenges, an affordable, easily synthesized, and environmentally friendly single amino acid bionanozyme (F-Cu) have been engineered. This bionanozyme harnesses phenylalanine (F) and redox-active Cu^{2+} ions to create 2D hierarchical van der Waals crystals. The F-Cu nanosheets exhibit rapid and real-time POD-mimicking catalytic activity, efficiently reducing hydrogen peroxide (H_2O_2), and demonstrating robustness under extreme pH, long-term storage, and elevated temperatures. Additionally, the F-Cu bionanozyme facilitates user-friendly, sensitive, and specific equipment-free visual detection of biomarkers, including Hydrogen peroxide (H_2O_2), dopamine (DA), and nitrite ions (NO_2^-), with detection limits as low as 5, 1.5, and 4 µM, respectively. These results underscore the alignment of the F-Cu bionanozyme with the WHO-REASSURE standards and its potential to address the future requirements of point-of-care diagnostics, biotechnology, food safety, and analytical chemistry applications.

1. Introduction

The advancement of biosensing technologies, adhering to the REASSURE (Real-time connectivity, Ease of specimen collection, Affordable, Sensitive, Specific, User-Friendly, Rapid, and Robust, Equipment free or simple Environmentally friendly, Deliverable to end-users) criteria set by the World Health Organization (WHO), holds considerable promise for application in resource-limited settings.[1,2] These technologies are expected to have a profound impact on biomedical diagnostics, food safety, and environmental monitoring. One particularly fascinating area of focus is the development of biosensors specifically designed to detect important biomarkers such as hydrogen peroxide (H_2O_2),[3,4] Dopamine (DA),[5] and Nitrite ion (NO_2^-), ions.[6,7] H_2O_2 is known for its powerful oxidizing characteristics, which can present serious health risks through various exposure routes. Meanwhile, DA, a vital neurotransmitter, is closely linked to neurological functions, and fluctuations in its levels can be associated with conditions like Parkinson's and Alzheimer's. Additionally, accurate detection of nitrite (NO_2^-) levels in food items is crucial for preventing health risks associated with overconsumption, given that $NO_2^-$is commonly used in food preservation.[8,9] Hence, the development of advanced biosensors for detecting H_2O_2, DA, and NO_2^- not only promises to improve disease monitoring but also plays a vital role in ensuring food safety and quality, ultimately leading to significant improvements in overall human health and well-being.[10] In this regard, a pivotal element in biosensing technology is the utilization of peroxidase (POD) enzymes, renowned for their ability to catalyze the oxidation of diverse substrates through the reduction of H_2O_2 (**Figure 1a**).[11] This enzymatic activity underpins the development of sensitive and selective colorimetric assays, where the oxidation products induce noticeable color changes correlating with the concentration of target analytes.[12] Nevertheless, natural POD enzymes present several challenges.[13] They are costly to produce and purify, sensitive to harsh physical and chemical conditions, and lack operational stability. Moreover, natural

S. Vishwakarma, V. K. Patel, R. Shukla, P. Makam
Department of Chemistry
Indian Institute of Technology (BHU)
Varanasi, UP 221005, India
E-mail: pandeeswar.chy@itbhu.ac.in
O. S. Tiwari, E. Gazit
The Shmunis School of Biomedicine and Cancer Research
The George S. Wise Faculty of Life Sciences
Tel Aviv University
Tel Aviv 6997801, Israel
E-mail: ehudg@post.tau.ac.il

The ORCID identification number(s) for the author(s) of this article can be found under https://doi.org/10.1002/adfm.202502902

DOI: 10.1002/adfm.202502902

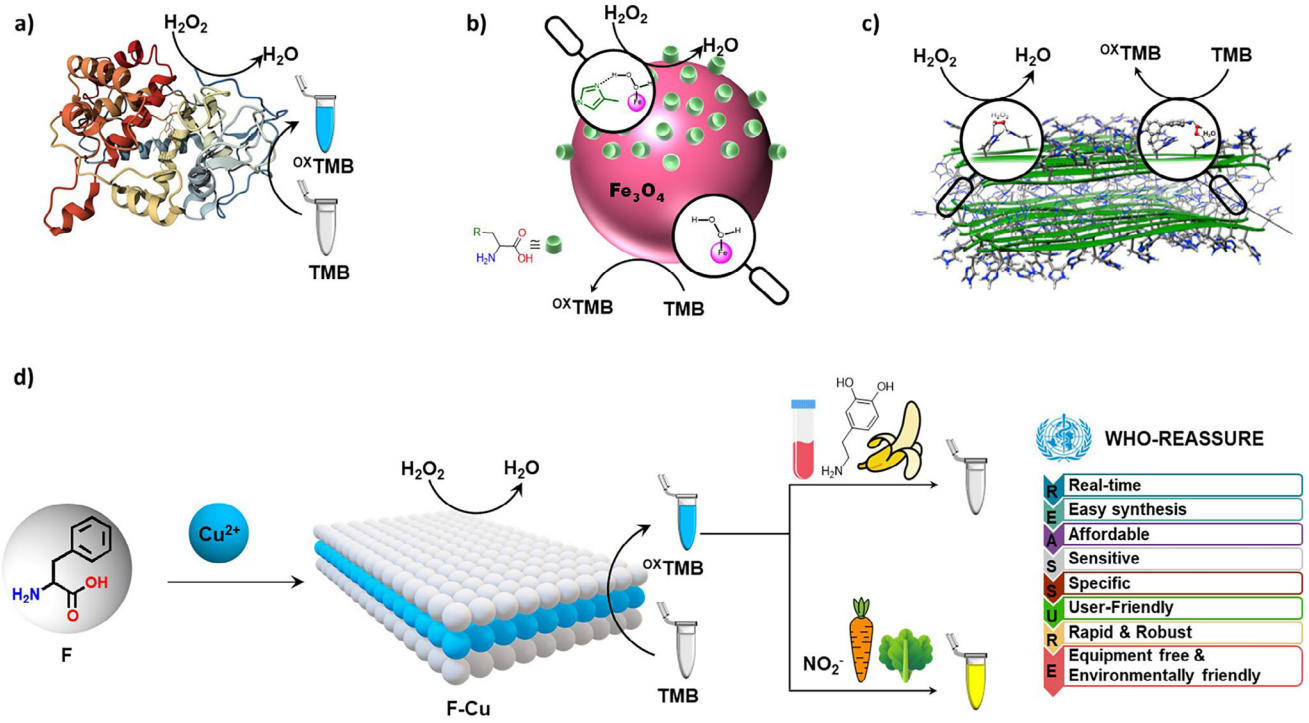

Figure 1. a) Structure and biocatalytic function of peroxidase (POD) enzyme (PDB: 1GZA; contains 344 amino acid protein sequence). b,c) presents previously reported POD mimicking amino acid-functionalized Fe_3O_4 nanozyme and cofactor-free bioinspired peptide-based bionanozyme. d) Schematic illustration of the development of single amino acid bionanozyme (F-Cu) presented in this report, showcasing its POD mimicking biocatalytic activity and its deployment as a colorimetric tool for biomarker detection, including H_2O_2 and DA (both test and real samples such as human blood serum, ripe banana peel) and NO_2^- ions (both test and real samples of spinach and carrot extracts) in accordance with WHO-REASSURE criteria.

enzymes pose difficulties in transferability, modification, recovery, and recyclability, necessitating the exploration of alternative biosensing methodologies. Recent advancements in nanotechnology have introduced nanozymes—nanomaterials that exhibit enzyme-like catalytic properties—as a promising solution to the shortcomings of natural enzymes.[14] Nanozymes offer several advantages, including enhanced stability and tunable catalytic activity, making them suitable candidates for biosensor development. Research efforts have primarily concentrated on replicating the functions of various oxidoreductase enzymes, such as POD, catalase, oxidase, and superoxide dismutase.[15] The pioneering work on POD-mimicking nanozymes began with the identification of Fe_3O_4 nanoparticles in 2007.[16] Subsequent studies revealed that specific Fe^{2+}-based nanocomposites could mimic POD activity by converting H_2O_2 into O_2 and hydroxyl radicals via the Fenton oxidation mechanism, exhibiting comparable catalytic efficiency and low substrate affinity. Notably, functionalizing the surface of Fe_3O_4 nanozymes with bioinspired amino acids significantly improved substrate affinity through hydrogen bonding interactions (Figure 1b).[17] To overcome the stability issues and narrow pH range activity of Fe^{2+}, researchers have explored the use of Cu^{2+} ions in developing POD-mimicking nanozymes via the Fenton-like reaction.[18,19] Despite these advancements, most nanozymes are inorganic-based nanomaterials, which significantly differ from the complex structure and properties of natural enzymes. This discrepancy hinders a thorough understanding of the enzymatic mechanisms and limits the rational design of artificial enzymes with predictable functionalities.[20] Additionally, the biomedical applications of these nanozymes are constrained by demanding synthetic conditions, complex fabrication processes, expensive equipment, toxic nature, and low specificity.

In response to these challenges, the development of bioinspired de-novo-designed catalytic biomolecular nanoassemblies, or bionanozymes, has emerged as a promising avenue.[21–23] Bionanozymes utilize biomolecules as building blocks, often in conjunction with cofactors, to mimic the structure and function of natural enzymes. This approach offers several advantages. First, the utilization of biomolecules enables the creation of bionanozymes with structures that closely resemble those of natural enzymes, potentially facilitating a more accurate understanding of enzymatic mechanisms.[24] Second, the design of bionanozymes can be more precise, allowing for the creation of artificial enzymes with specific functionalities tailored for desired applications. Significant progress has been made in developing peptide-based bionanozymes that replicate the active sites and catalytic features of various enzymes.[25] Recent research has notably demonstrated the development of cofactor-free peptide assemblies exhibiting POD-mimicking biocatalytic activity (Figure 1c).[26,27] Understanding the catalytic mechanisms of these bionanozyme systems is crucial for elucidating the structure-function relationships of natural enzymes and for the rational design of more efficient artificial enzymes. Building on these advancements, our research focuses on a further minimalistic approach to bionanozyme design.[28] Herein, we describe

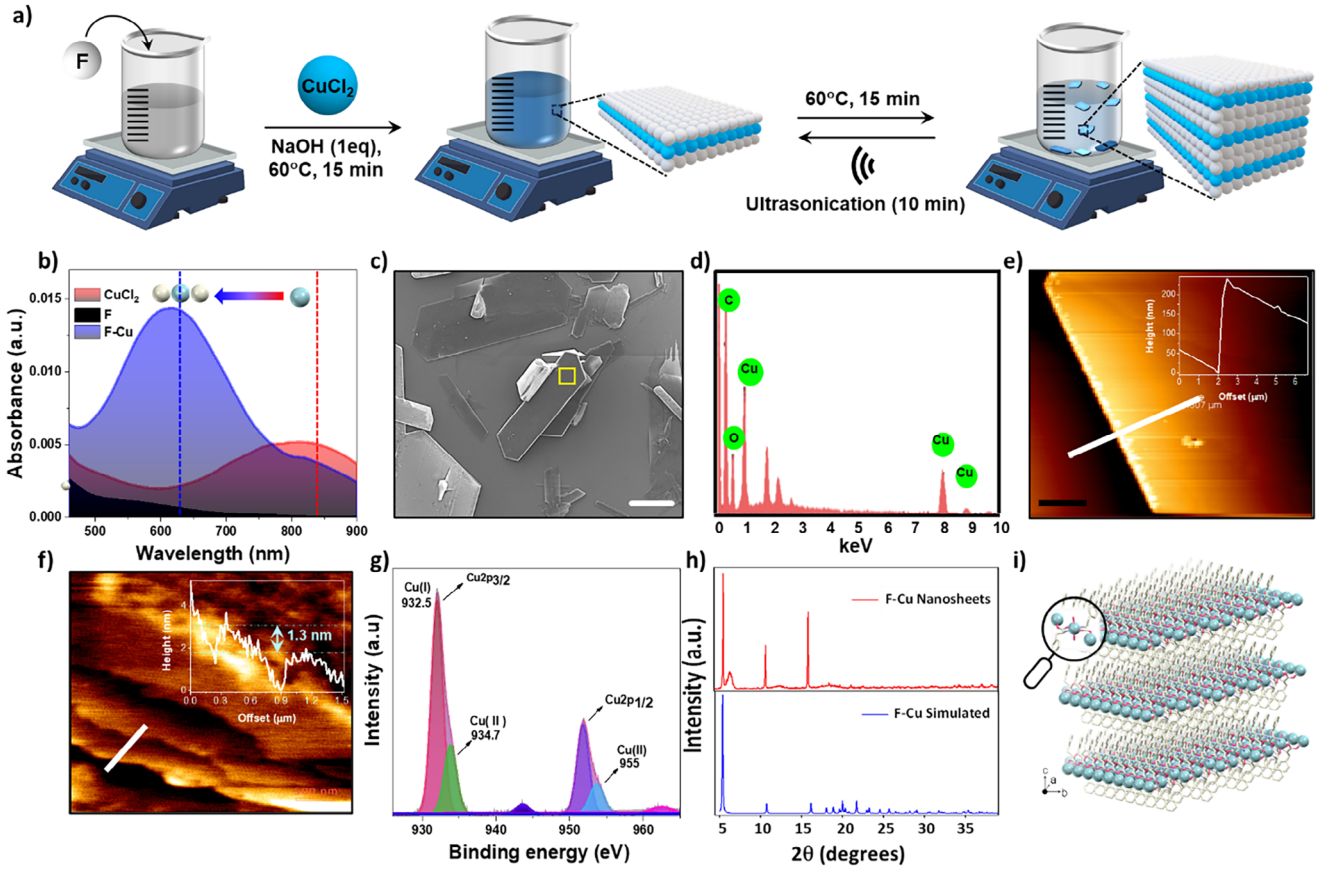

Figure 2. a) Schematic illustration of the synthesis of F-Cu bionanozyme. b) UV–vis absorption spectra of before and after (F-Cu) mixing of F and $CuCl_2$. c) HRSEM micrographs of F-Cu 2D microcrystals (scale bar 500 mm). d) EDX analysis on the selected area (yellow box in c) of the F-Cu microcrystal. e) AFM micrographs of pristine F-Cu 2D microcrystal and its height profile. f) AFM micrographs of ultrasonication-treated few layered F-Cu 2D nanosheets and their height profile. g) High-resolution XPS spectra of F-Cu nanosheets. h) Comparison of simulated PXRD patterns of F-Cu crystals with experimental PXRD of F-Cu nanosheets. i) The single-crystal X-ray structure of F-Cu crystal shows a layer-by-layer framework held together by interlayer van der Waals forces.[20]

the development of the simplest F-Cu bionanozyme that utilizes easily available and environmentally friendly single amino acid, phenylalanine (F), coordinated with Cu^{2+} ions to form ultrathin, 2D hierarchical layered crystals (Figure 1d). This simplest design leverages the redox-active (Cu^{2+}/Cu^{1+}) sites, making it a promising candidate for mimicking POD activity. Furthermore, we investigate the POD-like biocatalytic performance of the F-Cu bionanozyme and demonstrate its potential for developing WHO-REASSURE criteria-aligned ultrasensitive colorimetric sensing platforms for H_2O_2, DA, and NO_2^-.

2. Results and Discussion

2.1. Synthesis and Characterization of F-Cu Bionanozyme

The facile synthesis of a minimalistic POD-mimic was demonstrated by combining phenylalanine (F) with redox-active copper ions (Cu^{2+}) and examining the co-assembly process (**Figure** 2a). Notably, the initial interaction of F with $CuCl_2$ transformed the colorless alkaline reaction mixture into an intense blue solution, leading to the formation of blue-colored 2D crystals at the air-water interface. This transition was further analyzed through the UV–vis absorption spectra of the $CuCl_2$ aqueous solution, revealing a broad visible absorbance band at 820 nm. In contrast, F alone did not present significant visible bands, as shown in Figure 2b. However, the aqueous solution mixture of $CuCl_2$ and F exhibited a notably more intense, broader absorbance band, with a maximum wavelength (λ_{max}) at 615 nm.

This pronounced shift to a higher energy band at 615 nm, accompanied by a significant blue shift ($\Delta\lambda_{max}$ = 205 nm) relative to $CuCl_2$ alone, implies the induction of a t_{2g}-e_g transition through F-Cu complexation, characteristic of octahedral copper complexes undergoing tetragonal distortion attributable to the Jahn-Teller effect. Further insights into the morphology and composition of the synthesized F-Cu were obtained through high-resolution scanning electron microscopy (HRSEM) analysis of the drop-cast F-Cu complex solution, revealing the presence of 2D microcrystals (Figure 2c). Complementary energy-dispersive X-ray (EDX) analysis confirmed the integration of copper (Cu) along with carbon (C), nitrogen (N), and oxygen (O) (Figure 2d). Atomic force microscopy (AFM) topographic analysis provided a detailed view, showcasing multilayered hierarchical 2D sheets

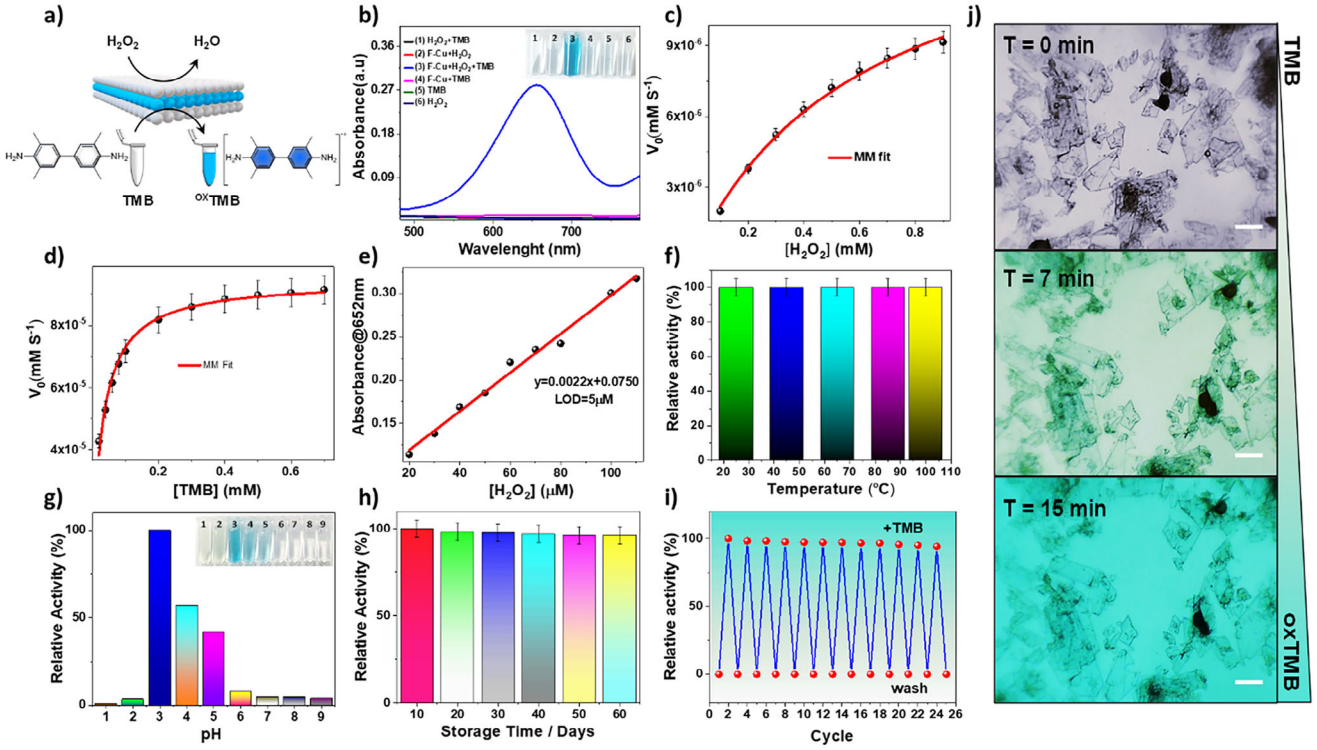

Figure 3. a) Schematic illustration of POD-mimicking biocatalytic activity of F-Cu bionanozyme. b) UV–vis absorption spectra of substrates in the presence of F-Cu bionanozyme and all the possible control combination studies. c, d) Initial rate (V_0) of the reaction catalyzed by F-Cu bionanozyme as a function of substrate [H_2O_2] (c) and [TMB] (d) concentration with Michaelis–Menten (MM) equation model fitting. e) Standard linear curve for the colorimetric detection of H_2O_2 in a linear concentration range of [H_2O_2] 20–110 μM, with LOD value 5 μM. f) Effect of temperature on the POD-like activity of F-Cu bionanozyme. g) Optimization of POD-like biocatalytic activity of F-Cu on varying ranges of pH [(Acidic (pH-1) to Alkaline (pH-9)]. h) Relative activity of F-Cu bionanozyme under different storage days (10–60 days). i) Recyclability of F-Cu, up to 12 cycles indicates its high stability during the course of POD-like activity. j) Optical microscopy snapshots at different intervals (0, 7, and 15 min) taken from the in situ reaction monitoring of H_2O_2 and TMB catalyzed by F-Cu bionanozyme (Movie S2, Supporting Information), the solution color change going from colorless (at 0 min) to blue (after 15 min) indicating the progress of catalytic reaction process.

spanning several micrometers in both length and width, with an average height of 230 nm (Figure 2e). Subsequent ultrasonication treatment yielded exfoliated few-layered 2D nanosheets, characterized by a single sheet thickness of ≈1.3 nm (Figure 2f). To delve deeper into the chemical composition and oxidation state of copper within the F-Cu 2D nanosheets, X-ray photoelectron spectroscopy (XPS) was employed. The XPS complete scan spectrum validated the presence of O, N, and C, with peaks at 532, 402, and 282 eV, respectively (Figure S1b–d, Supporting Information). The high-resolution XPS spectrum elucidated peaks at 932 and 951.8 eV, corresponding to the Cu 2p3/2 and Cu 2p1/2 electrons of Cu^{2+}, respectively (Figure 2g). Notably, the appearance of lower binding energy peaks at 932.5 and 955 eV signaled the presence of Cu^{+} (or Cu^{0}). Furthermore, the powder X-ray diffraction (PXRD) patterns of the synthesized F-Cu nanosheets exhibited significant congruence with the simulated PXRD patterns of F-Cu single crystals, indicating a similarity in crystallographic packing structures (Figure 2h).[20] Intriguingly, single-crystal X-ray crystallographic analysis revealed a graphite-like hierarchical infinite in-plane 2D F-Cu coordinated layer-by-layer framework, meticulously held together by interlayer van der Waals forces (Figure 2i).[20]

2.2. POD Mimicking Catalytic Characterization of F-Cu Bionanozyme and its REASSURE Aligned Detection of H_2O_2

2D layered nanomaterials have long been recognized as exceptional candidates for catalytic applications due to their unique structural and electrical properties.[29] In this study, we explored the POD-mimicking biocatalytic activity of F-Cu nanosheets in the presence of hydrogen peroxide (H_2O_2) by evaluating the oxidation of the benchmark POD substrate, 3,3′,5,5′-tetramethylbenzidine (TMB). As illustrated in **Figure 3**a, the catalytic reduction of H_2O_2 by F-Cu bionanozyme converts it into H_2O molecules, during this process the colorless TMB oxidizes to a deep blue chromogenic product (^{ox}TMB) with a characteristic absorbance at 652 nm, as depicted in Figure 3b and Movie S1 (Supporting Information).[30] Upon the addition of optimum concentration of F-Cu bionanozyme (0.1 mg mL^{-1} (optimization of F-Cu shown in Figure S3a, Supporting Information) to a colorless H_2O_2 and TMB reaction mixture in PBS (1X, pH 3, 24 °C), an immediate color change to deep blue is observed, accompanied by a broad absorbance band in the visible region with a maximum at 652 nm. This validates the intrinsic POD-mimicking biocatalytic capability of the F-Cu bionanozyme. In contrast, control

substrate solutions (H_2O_2, TMB, F-Cu alone, and combinations of H_2O_2+TMB, H_2O_2+F-Cu, and TMB+F-Cu) did not exhibit any significant visible color change or absorbance band, indicating the absence of background reactions (inset photograph, Figure 3b). Next, identical experiments were performed in the acetate buffer as well, interestingly results suggested more activity in the PBS buffer as compared to the acetate buffer (Figure S2a, Supporting Information). To elucidate the reaction kinetics, the reaction rates were measured under constant catalyst concentration (0.1 mg mL^{-1}) while systematically varying the concentrations of H_2O_2 and TMB. The enzyme-like kinetics of the F-Cu bionanozyme are evident in the relationship between the initial reaction rate and substrate concentration for both H_2O_2 and TMB, as shown in Figure 3c,d, respectively. Initially, an exponential increase in reaction rate is observed, which subsequently plateaus, indicating that further increases in substrate concentration do not significantly impact the reaction rate (Figure S3b,c, Supporting Information). The initial reaction velocity in relation to substrate concentration aligns well with the Michaelis-Menten (MM) equation, a fundamental model in enzyme kinetics. From the MM fitting analysis, we extracted the maximum reaction rate (V_{max}) and the Michaelis-Menten constant (K_m), which were then compared with literature values (Table S1, Supporting Information). For H_2O_2 as the substrate, F-Cu exhibits kinetic parameters with a V_{max} of 1.71×10^{-5} мм s^{-1}, K_m of 0.718 мм and K_{cat} of 3.41/s Similarly, with TMB as the substrate, the F-Cu bionanozyme demonstrated a V_{max} of 9.3×10^{-5} мм s^{-1}, a K_m of 0.0272 мм and a K_{cat} of 18.5/s comparable to those reported for the natural enzyme horseradish peroxidase (HRP) ($V_{max} = 10 \times 10^{-5}$ мм s^{-1} and $K_m = 0.434$ мм).[16] Notably, the lower K_m values for F-Cu bionanozymes indicate a higher substrate binding affinity compared to HRP enzymes.

To investigate the reaction mechanism involved in the catalytic reduction of H_2O_2 by the F-Cu bionanozyme, we analyzed the fluorescence characteristics of terephthalic acid (TA), a well-established probe in this context. TA, a non-fluorescent compound, undergoes oxidation to form the highly fluorescent O-Hydroxy Terephthalic acid (HTA) in the presence of •OH radicals, rendering it an effective fluorescent probe for detecting of in-situ generated •OH radicals. Subsequent to initiating the reaction, TA exhibited a new broad fluorescence emission band centered at 420 nm, indicative of HTA formation (Figure S4a,b, Supporting Information). This observation confirms the generation of •OH radicals during the F-Cu bionanozyme-catalytic reduction of H_2O_2. While the reaction progressed, the fluorescence emission band at 420 nm steadily increased, signifying a gradual escalation in the •OH intermediate content. This investigation confirms the proficient catalysis of the reduction of H_2O_2 into •OH radicals by the F-Cu bionanozyme, resembling the behavior of the POD enzyme. These radicals subsequently oxidize TA, resulting in the formation of the fluorescent HTA product. Furthermore, a series of experiments was conducted to gain insights into the reaction intermediates. Notably, reactive oxygen species (ROS) such as superoxide radicals ($O_2^{\bullet-}$) and •OH radicals were selectively scavenged using p-benzoquinone (PBQ) and isopropanol (IPA), respectively.[31–33] Following the co-incubation of F-Cu, H_2O_2, and TMB with PBQ, IPA, and a combination of both (IPA+PBQ), a substantial reduction in relative activity was observed with IPA+PBQ (Figure S5a, Supporting Information). In comparison, the samples with IPA and PBQ exhibited approximate declines of 50% and 10%, respectively. These findings suggest that both •OH and $O_2^{\bullet-}$ contribute to the oxidation of TMB, confirming the F-Cu bionanozyme Fenton-like catalytic mechanism (Figure S5a, Supporting Information). Additionally, a comparative study was conducted to evaluate the catalytic activity of POD-mimicking complexes using various metal combinations: F-Zn, F-Cu, F-Co, and F-Ni. Notably, the non-copper complexes (F-Zn, F-Co, F-Ni) displayed minimal catalytic activity (Figure S2b, Supporting Information). This finding can be attributed to copper's distinct electronic configuration and its redox behavior, which enable effective reactive oxygen species (ROS) generation.[34] These results suggest that the unique properties of copper play a crucial role in the catalytic performance of F-Cu bionanozyme. The absorbance of ^{ox}TMB at 652 nm is directly proportional to the concentration of H_2O_2, enabling the quantitative assessment of H_2O_2 based on the catalytic activity of the F-Cu bionanozyme. The absorbance intensity at 652 nm increased progressively with the H_2O_2 concentration, ranging from 0 to 110 µм (Figure S6). This change was also visually apparent, transitioning from colorless to blue, providing an immediate visual indication. Within the concentration range of 20–110 µм, a linear relationship was observed, allowing the calculation of the limit of detection (LOD) for H_2O_2 to be 5 µм (Figure 3e). This LOD is comparable to or surpasses those reported in previous studies (Table S2, Supporting Information). These findings highlight the efficacy of the colorimetric detection of H_2O_2 leveraging the POD-mimicking activity of the F-Cu bionanozyme.

In practical applications, the stability of a catalyst within industrial settings is of paramount importance. To evaluate the stability of the F-Cu bionanozyme in the catalytic reduction of H_2O_2 under extreme conditions, a series of experiments were conducted. Thermal stability was first assessed by incubating F-Cu at temperatures ranging from 0 to 110 °C for 40 min, followed by conducting a catalytic activity assay at room temperature (Figure 3f). Remarkably, the F-Cu bionanozyme demonstrated exceptional thermal stability, maintaining over 95% relative activity across a wide temperature range (20–110 °C). In contrast, the natural enzyme HRP exhibited a gradual decline in activity beyond 30 °C due to thermal denaturation, culminating in complete loss of function at ≈65 °C.[35] To determine the optimal pH for catalysis, the F-Cu catalytic assay for H_2O_2 reduction was performed at various pH levels from 1 to 9 (Figure 3g). The highest relative activity was observed at pH 3. As pH increased from 4 to 9, the catalytic activity of the F-Cu bionanozyme progressively decreased, indicating that an acidic environment with a pH of 3 is optimal for H_2O_2 reduction. This demonstrates the pH-dependent catalytic activity of the F-Cu bionanozyme: at pH 3, it exhibits POD-like activity, while at neutral pH 7, it shows laccase-like activity by oxidizing phenols.[20] The storage stability of the F-Cu bionanozyme was evaluated by incubating it in double-distilled water at 25 °C, with catalytic activity measured every ten days over two months (Figure 3h). The F-Cu bionanozyme retained ≈97.6% and 96.2% of its relative activity after 30 and 60 days, respectively, demonstrating remarkable storage stability. Recyclability was assessed by performing the H_2O_2 catalytic assay, isolating the F-Cu bionanozyme via centrifugation at 12 000 rpm for 10 min after each cycle, and rinsing with double-distilled water before reuse. The F-Cu bionanozyme maintained over 94% of its

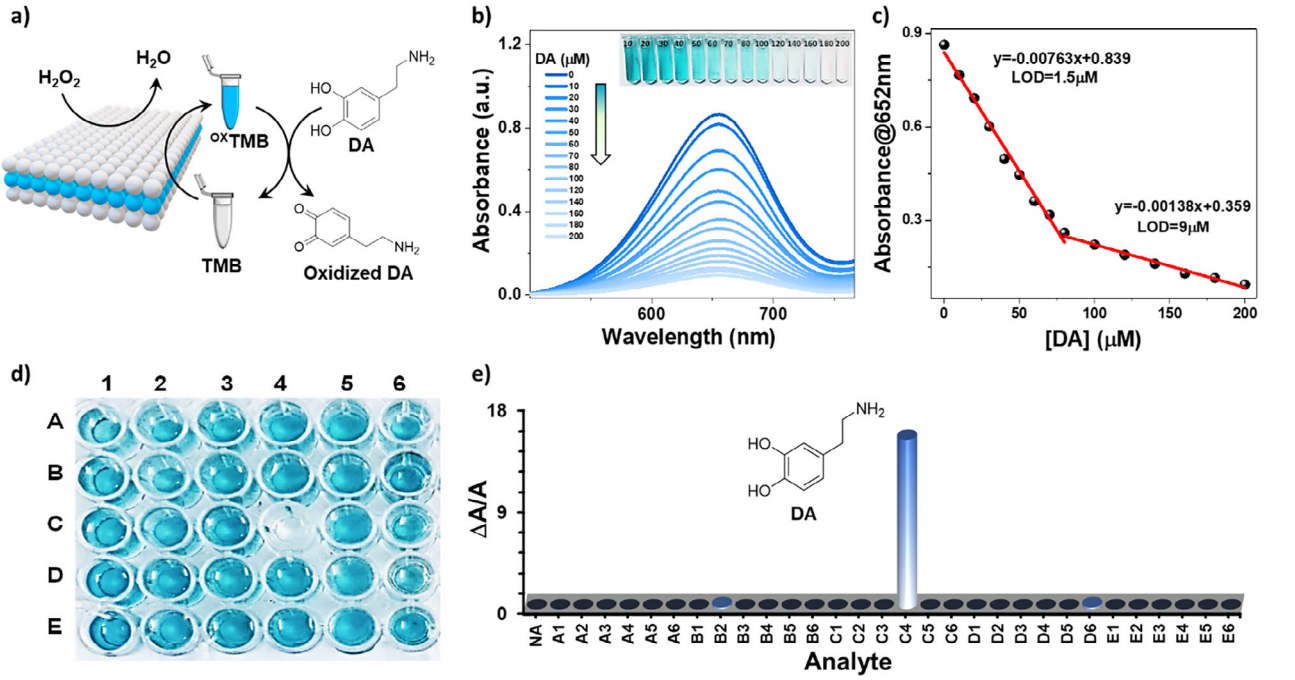

Figure 4. a) Schematic representation of the DA detection process facilitated by the POD mimicking F-Cu bionanozyme. b) UV–vis absorption spectra show the change in ^{ox}TMB absorbance with increasing concentrations of DA from 0 to 200 μM. c) The calibration curves for DA concentration range from 0 to 80 μM and from 80 to 200 μM, with the limits of detection (LOD) specified as 1.5 μM for the lower range and 9 μM for the higher range, derived from linear regression analysis. d) The photograph of a microwell plate with various analytes reacting in a mixture of F-Cu, H_2O_2, and TMB, highlights the equipment-free visual detection capability for DA (specifically in well C4), as indicated by the color change from blue to colorless (A1 = L-Phenylalanine, A2 = L-Lysine, A3 = L-Histidine, A4 = L-Proline, A5 = L-Serine, A6 = L-Tryptophan, B1 = L-Tyrosine, B2 = L-Cysteine, B3 = L-Glutamic acid, B4 = L-Arginine, B5 = L-Aspartic acid, B6 = Glycine, C1 = L-Alanine, C2 = L-Valine, C3 = L-Isoleucine, C4 = DA, C5 = L-Methionine, C6 = D-Glucose, D1 = L-Leucine, D2 = L-Threonine, D3 = L-Asparagine, D4 = Uric Acid, D5 = L-Glutamine, D6 = Ascorbic acid, E1 = Mn^{2+}, E2 = Co^{2+}, E3 = Zn^{2+}, E4 = K^+, E5 = Na^+, E6 = Cu^{2+}). Each interfering analyte was tested at a concentration of 200 μM. e) The corresponding net absorbance change (ΔA/A) at 652 nm for each analyte, underscores the selective response towards DA (well C4).

relative catalytic activity after twelve reuse cycles (Figure 3i). In situ microscopy was utilized to observe the stability and surface activity of the F-Cu bionanozyme during the catalytic H_2O_2 assay, with observations recorded at 15-s intervals over 30 min (Movie S2, Supporting Information). Initially, the reaction solution was colorless, along with 2D F-Cu bionanozyme crystals. As the reaction proceeded, the solution developed a pronounced blue hue without altering the underlying 2D morphology of the F-Cu bionanozyme crystals (Figure 3j). This observation confirms the stability of the F-Cu bionanozyme, with catalytic activity localized at the crystal surface. Filtration tests further supported these findings by separating the F-Cu bionanozyme from the reaction mixture and conducting the H_2O_2 catalytic assay using the filtrate. The filtrate did not show significant color change, indicating that the catalytic activity is exclusively attributable to the F-Cu bionanozyme (Figure S3d, Supporting Information). These rule out the possibility of Cu^{+2} ion release or the involvement of dissolved or non-assembled structures in the filtrate as contributing factors.

3. POD-Mimicking F-Cu Bionanozyme Mediated Visual Detection of Dopamine

Having successfully demonstrated the remarkable POD-mimicking capability of the F-Cu bionanozyme, our research focus shifted to exploring its potential for dopamine (DA) detection, as depicted in **Figure** 4a (Figure S7a, Supporting Information). The solution of the F-Cu bionanozyme system (F-Cu+H_2O_2+TMB) displayed a transition from colorless to deep blue, as indicated by the ^{ox}TMB absorption band at 652 nm in the absence of DA. Intriguingly, with the introduction of DA, the intense blue color diminished, restoring the solution to a colorless state (Movie S3, Supporting Information). The photographic evidence and absorption spectra in Figure 4b, depicting the impact of varying DA concentrations (ranging from 0 to 200 mM), unveiled a discernible correlation between DA concentration, the fading of the blue-colored solution, and the gradual decline of the corresponding ^{ox}TMB absorption band at 652 nm. This confirmed the DA-induced reduction of ^{ox}TMB to TMB. Furthermore, the calibration curve of absorbance versus DA concentration exhibited linearity within the ranges of 0–80 μM (R^2 = 0.99) and 80–200 μM (R^2 = 0.9469), suggesting distinct reaction states of DA (Figure 4c). The calculated DA limit of detection (LOD) was as low as 1.5 and 9 μM within the respective linear regimes, indicating the ultra-sensitivity of the POD-mimicking F-Cu bionanozyme system in comparison to prior reports (Table S3, Supporting Information). To assess the DA selectivity of the F-Cu bionanozyme system, interference experiments were conducted in the presence of various analytes including amino acids, metal ions, and a few metabolites. Figure 4d,e signify the

Table 1. F-Cu bionanozymes mediated DA detection from real sample extracts.

Sample	Spiked [DA] [μM]	Total [DA] spiked [μM]	Detected [DA] [μM]	% Error
Blood Serum	0	0	0	NA
	10	10	9.95	0.5
	10	20	20.21	1.05
	10	30	29.74	0.86
Ripped Banana Peel	0	0	0	NA
	10	10	10.21	2.10
	10	20	20.18	0.90
	10	30	30.14	0.46
Dopamine Injection	0	0	10	NA
	10	10	20.08	0.40
	10	20	30.67	2.23
	10	30	40.61	1.52

distinct color changes and relative identification efficiency of DA, suggesting its pronounced impact compared to other substances. This infers that DA selectively reduces the ^{ox}TMB back to TMB. This remarkable selectivity is attributed to dopamine's specific chemical structure, which includes multiple hydrogen atoms on its aromatic ring that enhance electron density and mobility, aiding in the capture of •OH radicals (Figure S7b, Supporting Information).[36] Moreover, the practical applicability of the F-Cu bionanozyme system was evaluated through the detection of DA in real samples, including human blood serum, ripped banana peel, and commercially available dopamine hydrochloride injection.[37,38] Using the standard addition method, the concentrations of DA in the aforementioned samples were determined to be 0 μM, 0 μM, and 10 μM, respectively (Table 1; Figure S8a–c, Supporting Information). Additionally, spiked DA experiments demonstrated accurate detection in all the real samples with less than 10% error. The combined results indicate that the F-Cu bionanozyme system designed to mimic POD catalytic activity shows promise as an exceptionally sensitive and selective colorimetric DA sensor. This suggests the potential for diverse applications in biomedical diagnostics (**Table 1**).

4. POD-Mimicking F-Cu Bionanozyme Mediated Visual Detection of Nitrite (NO_2^-)

Interestingly, it was observed that the addition of nitrite (NO_2^-) altered the color of the F-Cu bionanozyme system (F-Cu+H_2O_2+TMB) solution (Figure S9, Supporting Information). As shown in **Figure 5a**, the F-Cu bionanozyme system initially exhibits a blue color due to the POD mimicking catalytic oxidation of TMB. Upon the addition of a small amount of NO_2^- (100 μM), the solution's color transitions from blue to yellow (Movie S4, Supporting Information). Correspondingly, the UV–vis absorption signal at 652 nm, attributed to ^{ox}TMB, decreases in the presence of NO_2^-, while a newdemon significant signal appears at ≈445 nm (Figure 5b). This phenomenon can be attributed to the reaction between ^{ox}TMB and NO_2^-. The aromatic primary amine group in ^{ox}TMB reacts with NO_2^- in an acidic environment (pH 4) to undergo a typical diazotization reaction.[7] Consequently, the consumption of blue ^{ox}TMB reduces the original signal at 652 nm and the formation of yellow colored product is the colorimetric signal for the nitrite ion detection. Next, Figure 5c demonstrates the impact of varying concentrations of NO_2^- (0–140 μM). Furthermore, the calibration curve of absorbance versus NO_2^- concentration exhibited linearity within the range of 0–60 μM (R^2 = 0.99) (Figure 5d). The calculated limit of detection (LOD) for NO_2^- was as low as 4 μM, indicating the ultra-sensitivity of the F-Cu bionanozyme system as compared to the prior reports (Table S4, Supporting Information). Crucially, the cascade of POD-mimicking catalysis and diazotization demonstrates high specificity toward nitrite. Figure 5e compares the responses of various interfering analytes, including amino acids, metal ions, and certain metabolites, to the F-Cu bionanozyme system. The results indicate that only NO_2^- triggers the generation of the signal at 445 nm, highlighting the system's excellent selectivity toward the target analyte. This specificity forms the basis for NO_2^- detection. To evaluate the feasibility of the F-Cu bionanozyme system for detecting NO_2^- in real samples, we analyzed NO_2^- in commonly consumed green vegetables such as carrots and spinach.[8] A well-established procedure was employed to extract nitrite ions from carrots and spinach, and the detection assay was conducted.[7,39] Interestingly, NO_2^- was detected in carrot and spinach extracts at ≈0 and 0 μM, respectively (Figure S10a,b, Supporting Information; **Table 2**). Moreover, spiked experiments demonstrated less than 7% error in detecting NO_2^- ions in real samples, suggesting the system's practical applicability. Hence, the F-Cu bionanozyme system for catalytic detection of NO_2^- is anticipated to have potential applications in food safety monitoring and other relevant fields.

5. Sequential Detection of Analytes using F-Cu Bionanozyme-Based Logic Gate Systems

This study describes a unique approach for the sequential detection of analytes employing a logic gate-inspired F-Cu bionanozyme system (**Figure 6**). By leveraging the colorimetric properties of chromogenic substrates, this system enables visually

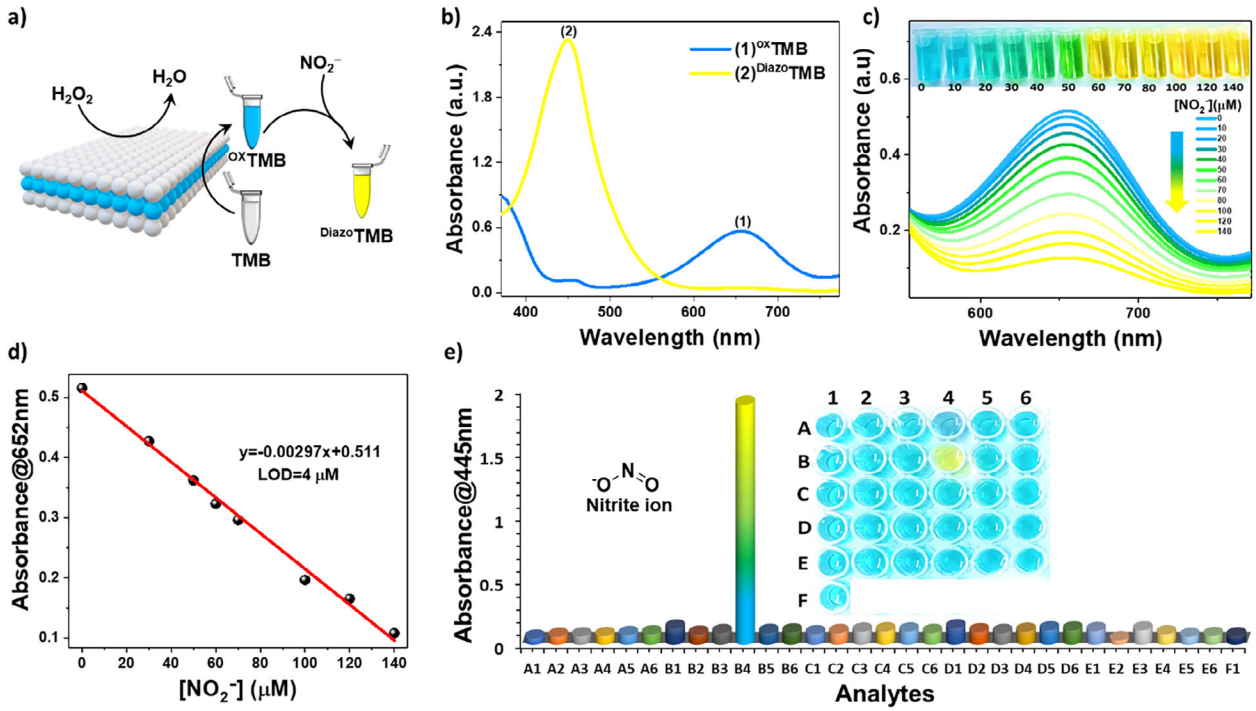

Figure 5. a) Schematic representation of the mechanism for NO_2^- detection mediated by F-Cu bionanozymes. b) UV–vis absorption spectra show the transformation of oxTMB to DiazoTMB in the presence of NO_2^-, highlighted by the emergence of a new absorption band at 445 nm. c) UV–vis spectra demonstrating the effect of increasing concentrations of NO_2^- (ranging from 0 to 140 μM) on oxTMB. d) Calibration curve depicting the linear response of NO_2^- ion concentration (0–140 μM) at an absorbance of 652 nm, with a calculated limit of detection (LOD) of 4 μM based on linear regression analysis. e) Comparative analysis of absorbance changes at 445 nm in the presence of various interfering analytes (A1 = L-Phenylalanine, A2 = L-Lysine, A3 = L-Histidine, A4 = L-Proline, A5 = L-Serine, A6 = L-Tryptophan, B1 = L-Tyrosine, B2 = L-Cysteine, B3 = L-Glutamic acid, B4 = NO_2^-, B5 = L-Aspartic acid, B6 = Glycine, C1 = L-Alanine, C2 = L-Valine, C3 = L-Isoleucine, C4 = DA, C5 = L-Methionine, C6 = D-Glucose, D1 = L-Leucine, D2 = L-Threonine, D3 = L-Asparagine, D4 = L-Glutamine, D5 = Mn^{2+}, D6 = Co^{2+}, E1 = Zn^{2+}, E2 = K^+, E3 = Na^+, E4 = Cu^{2+}, E5 = NO_3^-, E6 = SO_4^{2-}, F1 = PO_4^{3-}), showcasing the exceptional selectivity of the assay towards NO_2^- (B4). Each interfering analyte was tested at a concentration of 140 μM. Inset: A photograph of a microwell plate demonstrating the assay's capability for equipment-free, visually distinct detection of NO_2^-, as evidenced by a selective color change to yellow in well B4.

identifiable and sequential detection of target molecules through distinct color changes. The methodology mimics the operation of logic gates, where specific combinations of inputs result in predefined outputs. Here, analytes are designated as input signals (e.g., Input A and Input B), and the colorimetric responses represent output signals (e.g., Output Z). Logic Gate Design for H_2O_2 and DA Detection (Figure 6a,b): The system employs F-Cu bionanozyme to detect hydrogen peroxide (H_2O_2, Input A) and dopamine (DA, Input B). In this process, Input A (H_2O_2) triggers the reaction with TMB substrate in the presence of F-Cu bionanozyme, producing a blue-colored product (oxTMB). This signifies Output Z = 1, visually indicating the presence of H_2O_2. Input B (DA), when introduced after H_2O_2, reduces oxTMB to its colorless form, effectively turning Output Z = 0. This output change signifies the presence of DA. The corresponding truth table (Figure 6b) reflects the NOT-NOR logic gate functionality (NOT Gate: Inverts the input signal; NOR Gate: Outputs 1 only when both inputs are 0), where the initial output Z = 1 confirms H_2O_2 detection, and the transition to Z = 0 upon DA introduction indicates its presence. The absence of either analyte results in no

Table 2. F-Cu bionanozymes mediated NO_2^- detection from real sample extracts.

Sample	Spiked $[NO_2^-]$ [μM]	Total $[NO_2^-]$ [μM]	Detected $[NO_2^-]$ [μM]	% Error
Carrot	0	0	0	NA
	10	10	10.21	2.10
	10	20	21.05	5.25
Spinach	0	0	0	NA
	10	10	9.5	5.00
	10	20	21.4	7.00

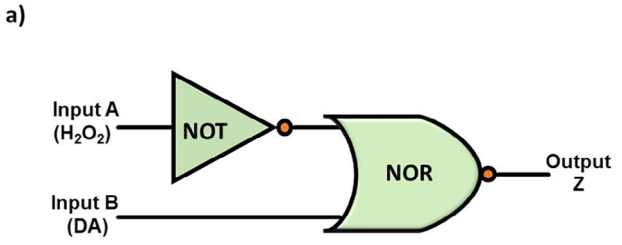

b)

Inputs		Output of NOT Gate	Output of NOR Gate (Z)	Colorimetric image
Input A (H_2O_2)	Input B (DA)			
0	0	1	0	
0	1	1	0	
1	0	0	1	
1	1	0	0	

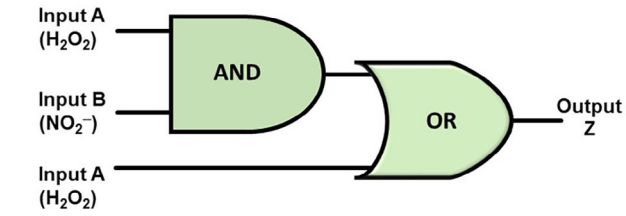

d)

Inputs		Output of AND Gate	Output of OR Gate (Z)	Colorimetric image
Input A (H_2O_2)	Input B (NO_2^-)			
0	0	0	0	
0	1	0	0	
1	0	0	1	
1	1	1	1	

Figure 6. Logic gate (a and c) and truth table (b and d) of the F-Cu bionanozyme system for the consecutive detection of H_2O_2 and DA (a and b) as well as H_2O_2 and NO_2^- (c and d).

color change (Z = 0), completing the NOT-NOR gate operation. Logic Gate Design for H_2O_2 and NO_2^- Detection (Figure 6c,d): Another implementation of the F-Cu bionanozyme logic gate involves the sequential detection of hydrogen peroxide (H_2O_2, Input A) and nitrite ions (NO_2^-, Input B). In this system, Input A (H_2O_2) reacts with TMB in the presence of F-Cu bionanozyme, forming oxTMB and producing a blue color (Output Z = 1). Input B (NO_2^-), introduced subsequently, reacts with oxTMB to form diazoTMB, leading to a yellow-colored product. The system retains Output Z = 1, indicating successful detection of both analytes. The truth table (Figure 6d) illustrates this AND-OR logic gate behavior (AND Gate: Outputs 1 only when both inputs are 1; OR Gate: Outputs 1 when at least one input is 1). The blue-to-yellow color change upon sequential introduction of NO_2^- validates its detection while confirming the presence of H_2O_2.

This logic gate-inspired colorimetric system offers several advantages, including simplicity, cost-effectiveness, and visual interpretability. Its potential applications span environmental monitoring, healthcare diagnostics, and food safety, where rapid and sequential analyte detection is critical. The user-friendly nature of this technique, coupled with the tunable properties of bionanozyme-based sensors, underscores its versatility in biosensing platform development.

6. Conclusion

In summary, we have successfully developed the simplest POD-mimicking single amino acid F-Cu bionanozyme system as an ultrasensitive colorimetric probe for detecting crucial biomarkers such as H_2O_2, dopamine, and nitrite ions. By leveraging the unique properties of F coordinated with Cu^{2+} ions, we synthesized F-Cu bionanozymes with a 2D hierarchical structure, featuring a dense arrangement of crystalline orderly redox-active (Cu^{2+}/Cu^{+}) accessible catalytic sites. The F-Cu bionanozyme demonstrates remarkable POD-like catalytic activity, capable of rapidly reducing H_2O_2 through a Fenton-like reaction mechanism while maintaining robustness under extreme pH variations, long-term storage, and elevated temperatures. Its ultrasensitive and rapid detection capabilities have been validated with detection limits as low as 5 µM for H_2O_2, 1.5 µM for DA, and 4 µM for nitrite ions. These outstanding performance characteristics align with the WHO-REASSURED criteria, making this bionanozyme a potential candidate for biosensing applications in resource-limited settings. These findings underscore the potential of bioinspired de novo-designed bionanozymes in overcoming the drawbacks associated with natural enzymes, including production costs, stability, and reusability. The minimalistic approach of utilizing a single amino acid and Cu^{2+} ions not only simplifies the synthesis process but also enhances the functional versatility and stability of the resulting bionanozyme. The implications of this research extend beyond immediate biosensing applications, laying the groundwork for the rational design of more sophisticated artificial enzymes. Our future endeavors will focus on the further refinement of bionanozyme design, the expansion of its range of applications, and its integration into practical diagnostic and monitoring devices. This initiative holds significant promise for a wide spectrum of applications in point-of-care diagnostics, biotechnology, environmental monitoring, food safety, and healthcare.

Supporting Information

Supporting Information is available from the Wiley Online Library or from the author.

Acknowledgements

P.M. acknowledged the support from ICMR, India (IIRPSG-2024-01-03827) and IIT (BHU). S.V. thanks the UGC-India and IIT (BHU) for the research fellowship. E.G. thanks to the Airforce research laboratories (AFRL) for support. This material is based on work supported by the Air Force Office of Scientific Research under award number FA8655-21-1-7004. Any opinions, findings, conclusions, or recommendations expressed in this material are those of the authors and do not necessarily reflect the views of the United States Air Force.

Conflict of Interest

The authors declare no conflict of interest.

Data Availability Statement

The data that support the findings of this study are available in the supplementary material of this article.

Keywords

analytical chemistry, biomarkers, bionanozyme, biosensors, biotechnology, peroxidase, point-of-care diagnostics, two-dimensional (2D) crystals, WHO-REASSURE criteria

Received: January 30, 2025
Revised: May 26, 2025
Published online: June 8, 2025

[1] K. J. Land, D. I. Boeras, X.-S. Chen, A. R. Ramsay, R. W. Peeling, *Nat. Microbiol.* **2018**, *4*, 46.
[2] M. Zandieh, J. Liu, *Adv. Mater.* **2024**, *36*, 2211041.
[3] Q. Shi, Y. Song, C. Zhu, H. Yang, D. Du, Y. Lin, *ACS Appl. Mater. Interfaces* **2015**, *7*, 24288.
[4] Y. Mirzaei, A. Gholami, A. Sheini, M. M. Bordbar, *Sci. Rep.* **2023**, *13*, 7064.
[5] P. K. Boruah, P. Borthakur, G. Neog, B. Le Ouay, N. U. Afzal, P. Manna, M. R. Das, *ACS Appl. Nano Mater.* **2023**, *6*, 1667.
[6] M. Ayala, E. Torres, in *Heme Peroxidases*, The Royal Society of Chemistry, London, UK **2015**, pp. 309–333.
[7] J. Liu, L. Gong, H. Chen, J. Gui, X. Zhu, M. Liu, Y. Zhang, S. Yao, *ACS Appl. Nano Mater.* **2023**, *6*, 5879.
[8] S. Luetic, Z. Knezovic, K. Jurcic, Z. Majic, K. Tripkovic, D. Sutlovic, *Foods* **2023**, *12*, 1655.
[9] B. Kgedal, D. S. Goldstein, *J. Chromatogr. B Biomed. Sci. Appl.* **1988**, *429*, 177.
[10] L. Su, S. Qin, Z. Xie, L. Wang, K. Khan, A. K. Tareen, D. Li, H. Zhang, *Coord. Chem. Rev.* **2022**, *473*, 214784.
[11] X. Zhang, X. Chen, Y. Zhao, *Nano-Micro Lett.* **2022**, *14*, 95.
[12] Y. Gao, K. Wu, H. Li, W. Chen, M. Fu, K. Yue, X. Zhu, Q. Liu, *Sensors Actuators, B Chem.* **2018**, *273*, 1635.
[13] T. L. Poulos, *Chem. Rev.* **2014**, *114*, 3919.
[14] H. Wei, E. Wang, *Chem. Soc. Rev.* **2013**, *42*, 6060.
[15] A. M. Ashrafi, Z. Bytesnikova, J. Barek, L. Richtera, V. Adam, *Biosens. Bioelectron.* **2021**, *192*, 113494.
[16] L. Gao, J. Zhuang, L. Nie, J. Zhang, Y. Zhang, N. Gu, T. Wang, J. Feng, D. Yang, S. Perrett, X. Yan, *Nat. Nanotechnol.* **2007**, *2*, 577.
[17] N. Salarizadeh, M. Sadri, R. H. Sajedi, *Appl. Organomet. Chem.* **2018**, *32*, 4018.
[18] X. Geng, X. Xie, Y. Liang, Z. Li, K. Yang, J. Tao, H. Zhang, Z. Wang, *ACS Omega* **2021**, *6*, 6284.
[19] M. Fang, R. Zheng, Y. Wu, D. Yue, X. Qian, Y. Zhao, Z. Bian, *Environ. Sci. Nano* **2019**, *6*, 105.
[20] P. Makam, S. S. R. K. C. Yamijala, V. S. Bhadram, L. J. W. Shimon, B. M. Wong, E. Gazit, *Nat. Commun.* **2022**, *13*, 1505.
[21] X. Li, Y. Zhang, W. Tan, P. Jin, P. Zhang, K. Li, *Anal. Chem.* **2023**, *95*, 2865.
[22] D. Banerjee, S. Vishwakarma, M. Nayak, A. Upadhyay, L. Pradhan, P. Makam, S. Mukherjee, *ACS Appl. Nano Mater.* **2025**, *8*, 4263.
[23] S. Vishwakarma, O. S. Tiwari, R. Shukla, E. Gazit, P. Makam, *Chem. Soc. Rev.* **2025**, *54*, 465.
[24] Q. Liu, A. Kuzuya, Z. G. Wang, *iScience* **2023**, *26*, 105831.
[25] E. Dikici, B. Önal Acet, T. Gök, Ö. Acet, M. Odabaşi, *MANAS J. Eng.* **2023**, *11*, 83.
[26] Q. Liu, K. Wan, Y. Shang, Z. G. Wang, Y. Zhang, L. Dai, C. Wang, H. Wang, X. Shi, D. Liu, B. Ding, *Nat. Mater.* **2021**, *20*, 395.
[27] I. W. Hamley, *Biomacromolecules* **2021**, *22*, 1835.
[28] P. Makam, S. S. R. K. C. Yamijala, K. Tao, L. J. W. Shimon, D. S. Eisenberg, M. R. Sawaya, B. M. Wong, E. Gazit, *Nat. Catal.* **2019**, *2*, 977.
[29] D. Deng, K. S. Novoselov, Q. Fu, N. Zheng, Z. Tian, X. Bao, *Nat. Nanotechnol.* **2016**, *11*, 218.
[30] T. Tsuneda, *Sci. Rep.* **2020**, *10*, 18144.
[31] W. Cao, P. Ju, Z. Wang, Y. Zhang, X. Zhai, F. Jiang, C. Sun, *Spectrochim. Acta Part A Mol. Biomol. Spectrosc.* **2020**, *239*, 118499.
[32] S.-J. Yin, G.-Y. Chen, C.-Y. Zhang, J.-L. Wang, F.-Q. Yang, *Microchim. Acta* **2023**, *190*, 25.
[33] W. Song, P. Sun, J. Zhou, X. Han, Q. Dai, F. Chai, *New J. Chem.* **2023**, *47*, 15721.
[34] M. Marieeswaran, P. Panneerselvam, *Mater. Adv.* **2021**, *2*, 7024.
[35] T. Wang, J. Tian, T. Li, J. Li, *Atlantis Press* **2016**, 227.
[36] A. Slivka, G. Cohen, *J. Biol. Chem.* **1985**, *260*, 15466.
[37] X. Liu, J. Liu, *View* **2021**, *2*, 1.
[38] K. Kanazawa, H. Sakakibara, *J. Agric. Food Chem.* **2000**, *48*, 844.
[39] M. Wang, P. Liu, H. Zhu, B. Liu, X. Niu, *Biosensors* **2021**, *11*, 1.